Atmósfera (1993), 6, pp. 3 - 23

Impact of orographic gravity wave drag on extended–range forecasts with the COLA–GCM

B. KIRTMAN, A. VERNEKAR, D. DeWITT and J. ZHOU

Department of Meteorology, University of Maryland, College Park, Maryland 20742, USA

(Manuscript received March 17, 1992; accepted in final form June 16, 1992)

RESUMEN

El impacto del arrastre de las ondas de gravedad sobre el Modelo de Circulación General, del Centro para las Interacciones Océano–Tierra y Atmósfera, se estudia por simulación de dos pares de pronósticos de 30 días de plazo. Uno inicializado el 8 de enero de 1990 y el otro en julio 15 de 1989. Con cada condición inicial se elaboraron pronósticos con y sin efectos del arrastre de las ondas de gravedad. Los resultados muestran que los efectos del arrastre mejoran el pronóstico lo mismo en enero que en julio, especialmente en el hemisferio invernal. El arrastre reduce el sesgo del poniente en el viento zonal y el sesgo frío en la temperatura. Como consecuencia de los cambios en la cantidad de movimiento y la temperatura hay cambios en el transporte meridional de masa de tal modo que las presiones medias mensuales, al nivel del mar, mejoran particularmente en las regiones polares.

Más aún, a medida que el sesgo del poniente en la cantidad de movimiento es reducido la cantidad de movimiento del flujo de gran escala es llevado a la superficie de la Tierra donde se disipa. Este proceso de disipación aumenta el arrastre superficial efectivo y refuerza las circulaciones medias meridionales. Los resultados indican que éstas se incrementan en un 15% y la energía cinética divergente es aumentada en un 30% después del decimoquinto día. Asociada a las propias circulaciones secundarias se encuentra incrementada la precipitación promediada zonalmente en el hemisferio estival y disminuida la precipitación igualmente tratada en el hemisferio invernal en julio. En enero la precipitación aumenta en ambos hemisferios.

ABSTRACT

The impact of gravity wave drag (GWD) on the COLA (Center for Ocean–Land–Atmosphere Interactions) –GCM is studied by simulating two pairs of 30–day extended range forecasts. One is initialized on January 8, 1990, and the other on July 15, 1989. With each initial condition forecasts were made both with and without the GWD effects. The results show that GWD effects improve the forecast for both January and July particularly in the winter hemisphere. The GWD reduces the westerly bias in the zonal wind and the cold bias in the temperature. As a consequence of the changes in the momentum and temperature there are changes in the meridional mass transport such that monthly mean sea level pressures are improved particularly in the polar regions. Furthermore, as the westerly bias in the zonal momentum is reduced the momentum of the large scale flow is brought down to the Earth's surface where it is dissipated. This dissipation process increases the effective surface drag and enhances the mean meridional circulations. The results indicate that the mean meridional circulations are enhanced by 15% and the divergent kinetic energy is enhanced by 30% after day–15. Associated with the enhanced secondary circulations is increased zonally averaged precipitation in the summer hemisphere and decreased zonally averaged precipitation in the winter hemisphere in July. In January the precipitation increases in both hemispheres.

1. Introduction

Systematic errors in numerical weather prediction (NWP) models and "climate drift" in general circulation models (GCMs) have a coherent structure in space and time. They appear in zonally symmetic fields as well as in zonally asymmetric fields. The coherent structures of these error field are similar in several models irrespective of the differences in their treatment of dynamical

and physical processes. The systematic errors impair the ability of NWP models to forecast beyond a few days and the climate drift in the GCMs limits the reliability of simulating climate sensitivity to CO_2 doubling, sea surface temperature anomalies, deforestation or desertification. The degradation of dynamical extended range forecasts is also critically dependent on the systematic errors in the model. Therefore, it comes as no surprise that the problem of systematic errors and climate drift has recently received considerable attention from the scientific community.

It is believed that these systematic errors are largely due to subgrid scale processes. Recently, in companion articles Sirutis and Miyakoda (1990) and Miyakoda and Sirutis (1990) presented a comprehensive study on the impact of different parameterization schemes of subgrid scale processes on the systematic errors in the GFDL (Geophysical Fluid Dynamics Laboratory) model. Some of the most important subgrid scale processes identified by these authors were cloud–radiation interactions, planetary boundary layer processes, convection, exchange of heat, momentum, and water vapor between the Earth's surface and the atmosphere and subgrid scale orographic effects. Subgrid scale orographic effects are largely due to gravity waves generated when stably stratified air flows over subgrid scale orography. Eliassen and Palm (1961) and Bretherton (1969) have shown that when gravity waves of wave lengths larger than approximately 10 km are excited by irregular surface terrain they may propagate up to considerable altitudes before they are dissipated. These waves transport horizontal momentum upward and deposit this momentum where the waves are ultimately dissipated. At the level where the gravity waves dissipate or break the momentum is lost by the large–scale flow and is brought down to the Earth's surface where it is deposited. Lilly (1972) proposed that this process of dissipation and deposition of momentum due to gravity waves is important enough to include their effects explicity in NWP models and GCMs.

Observational studies have also shown that gravity waves of wave lengths exceeding 10 km propagate vertically and transport momentum between their source region and the regions where they are dissipated. A summary of the observations made over the Colorado Rocky Mountains was reported by Lilly *et al.* (1982). More recent observations over the British Isles were reported by Brown (1983) and over the Pyrenees were reported by Hoinka (1984). The magnitude of the observed estimates of the momentum flux due to gravity waves are in close agreement with the theoretically derived estimates. There is also observational evidence that dramatic increases in the surface drag occurs during wave breaking periods (Smith, 1978).

Lilly's proposal received attention only recently when new systematic errors were noted when the horizontal and vertical resolutions of both NWP models and GCMs were increased. In the low resolution models both the surface drag over the mountains and the horizontal flux of momentum, by explicitly resolved large scale eddies, were underestimated (Palmer *et al.*, 1986). In these low resolution models, initialized in winter, the simulated jet strength in the Northern Hemisphere agreed fairly accurately with observations, but in the Southern Hemisphere the jet strength was too weak. As the horizontal resolution increases so did the convergence of horizontal momentum flux due to the resolved large scale eddies. The increased momentum convergence results in improving the forecast of the jet strength in the Southern Hemisphere but produces a positive bias in the zonal mean winds in the Northern Hemisphere winter forecast. Associated with the westerly bias in the zonal wind were serious negative systematic errors in the temperature fields often exceeding 10°K in extensive regions of the upper troposphere. Boer *et al.* (1984) included the gravity wave drag (GWD) effects in a low resolution model to show that these effects reduce the strength of the westerly current and alleviate the low temperature bias. Palmer *et al.* (1986) were the first to show, in a high resolution model, that the effects of the GWD was of the appropriate magnitude to alleviate the positive bias in the westerly current. Similar results were shown by Helfand *et al.* (1987), McFarlane (1987), Stern and Pierrehumbert (1988), Alpert *et al.* (1988) and Iwasaki *et al.* (1989). While GWD schemes appear to improve forecasts initialized in winter, forecasts initialized in the summer months have not been previously investigated.

As mentioned above, when vertically propagating gravity waves were deposited, the momentum of the large scale flow is lost and brought down to the Earth's surface where it is dissipated. Smith (1979) speculated that this process will increase the effective surface drag and enhance the mean meridional circulations. Palmer *et al.* (1986) have demostrated this effect with the aid of a simple zonally averaged model. In addition, if the westerly bias is reduced by the dissipative effects of the gravity wave drag the north–south temperature gradient has to adjust such that the thermal wind balance is approximately maintained. This requires a meridional transfer of mass to compensate for the temperature change and in turn requires enhanced secondary circulations.

The effects of the gravity wave drag parameterization has been extensively studied in terms of medium range forecast (Helfand *et al.*, 1987; Alpert *et al.*, 1988 and Iwasaki *et al.*, 1989). Several GCM studies have also considered the gravity wave drag effects in climate simulations (see Palmer *et al.*, 1986 among others); however, there has been little investigation into the gravity wave drag effects on dynamical extended range forecasts. Furthermore, due to the large difference between summer and winter forecasts (or simulations) and their respective systematic errors it comes as no surprise that the impact of the enhanced drag should significantly differ between the seasons. The purposes of this study are threefold. First, include the gravity wave drag effect in a state–of–the–art GCM in order to reduce the temperature bias and zonal wind bias. Second, assess the differences in extended range forecasts initialized in January and July in the presence of the wave drag. Third, determine the magnitude of the enhanced divergent circulations associated with the enhanced drag. The first objective has been attempted while considering medium range forecasts and climate simulations but not in terms of extended range forecasts. To the best of our knowledge, the second and third objectives have not received any attention in the current literature.

We have made January and July extended range forecasts with the COLA (Center for Ocean–Land–Atmosphere Interactions) –GCM in the Department of Meteorology, University of Maryland, College Park. The forecasts were made both with and without the gravity wave drag effects. As we shall see, the GWD reduces the negative bias in the temperature beginning from day–1 of the forecast as well as the low sea level pressure bias in the high latitudes. In addition the GWD significantly enhances the mean meridional and divergent circulations and the associated precipitation. Section 2 provides a short description of the COLA-GCM. Section 3 outlines the gravity wave drag parameterization scheme adopted here. Section 4 briefly describes the experiments performed and presents the results from these experiments. Finally section 5 contains the summary and concluding remarks.

2. The COLA–GCM

The GCM is a global spectral model developed from the numerical weather prediction model described by Sela (1980). The horizontal variations of the fields are represented by rhomboidal truncation with a maximum total wave number of 40. The vertical variations are represented by 18 discrete sigma levels. The large scale barrier effects of the mountains are represented by the silhouette orography. The results of winter and summer forecasts based on an earlier version of the model were reported by Kinter *et al.* (1988).

The GCM incorporates a diurnal cycle, the shallow convection scheme of Tiedtke (1984), large scale precipitation, and the cumulus convection scheme comes from Kuo (1974). The planetary boundary layer which evolves freely in the model uses the parameterization of Mellor and Yamada (1982). The heat, water vapor and momentum transfer between the surface and the atmosphere is simulated by the biosphere model of Sellers *et al.* (1986). The transfer of momentum between the lowest model layer and the surface is based on the Monin–Obukhov similarity theory where the surface roughness length depends on the vegetation type and the

month. The layer between the surface and the lowest level is treated jointly as the surface layer, in which molecular as well as turbulent fluxes are combined, and a bulk transfer scheme is used. These frictional effects are only directly felt on the lowest layer in the model. The impact of the biosphere model on the hydrological cycle of the model was discussed by Sato *et al.* (1989).

The radiation scheme of Harshvardhan *et al.* (1987) is incorporated in this model and the cloud scheme is similar to the one developed by Slingo (1980, 1987). The model prescribes climatological sea surface temperature, sea ice extent and vegetation type. Soil moisture and snow cover are specified initially and predicted by the model. Diabatic non–linear normal mode initialization is used for making the 30–day forecasts.

3. The parameterization

The parameterization of gravity wave drag in numerical weather prediction and general circulation models is based on simplified theoretical concepts and observational evidence. The parameterization consists of determining the drag due to gravity waves at the surface and its vertical variation. We have adopted the scheme of Alpert *et al.* (1988). The parameterization of the drag at the surface is based on the formulation described by Pierrehumbert (1987) and the vertical variation of the drag is based on the schemes of Palmer *et al.* (1986) and Helfand *et al.* (1987).

The momentum flux due to the gravity waves averaged over a grid box is written as $\vec{\tau}_{gw} =< \rho \vec{V}' w' >$ where ρ is the density of air and $\vec{V}'$ and w' are respectively the fluctuations in the horizontal wind vector and vertical velocity due to gravity waves. The angle brackets indicate an average over the grid box. The GWD due to this momentum flux is then an additional body force on the atmosphere. That is,

$$\frac{\partial \vec{V}}{\partial t} + \ldots + = \frac{1}{\rho}\frac{\partial \vec{\tau}_{gw}}{\partial z} = -\frac{g}{p_s}\frac{\partial \vec{\tau}_{gw}}{\partial \sigma}. \tag{3.1}$$

Pierrehumbert (1987) argues that convective instability and wave breaking at the Earth's surface is so prevalent that nonlinear effects become very common and cannot be neglected. Based on scaling arguments and the results from numerical experiments, Pierrehumbert (1987) obtains a formula for the surface wind stress due to the gravity waves $\vec{\tau}_{gw}$. Pierrehumbert (1987) concludes that

$$\mid \vec{\tau}_{gw} \mid = \frac{\rho U^3}{N\ell^*}\left[\frac{F_r^2}{1+F_r^2}\right] \tag{3.2}$$

where $F_r = \frac{Nh}{U}$ is the Froude number, N is the Brunt–Vaisala frequency, U is the surface wind speed, h is the amplitude of the orographic perturbation, ℓ^* is the wave length of the monochromatic wave in the direction of the surface wind and $\vec{\tau}_{gw}$ is in the direction of the surface wind.

The equation (3.2) for the surface stress is valid for a wide range of values of the Froude number, in particular for $F_r < 0.8$ for which the linear theory is valid and for $F_r > 0.8$ nonlinear effects become important. On the other hand, the momentum flux due to the gravity waves above the breaking level increases linearly with Froude number even for $F_r > 0.8$. Assuming that the momentum flux due to the gravity waves does not change with height below the breaking level, the difference between the surface drag which equals $\vec{\tau}_{gw}$ below the breaking level and the

momentum flux due to the gravity waves above the breaking level is proportional to the wave–drag in the intervening layer. Consequently, in the nonlinear range, the momentum deposition within the breaking layer is much larger than in the linear range.

To account for the nonlinear amplification of the surface drag a base layer is defined to compute $\vec{\tau}_{gw}$ at the surface. The base layer is approximately the first one third of the model layer, in this case from the surface to 642 mb. Equation (3.2) is computed by using mass weighted variables over the depth of the base layer. In this study we have taken $\ell^* = 125$ km and h equals the subgrid scale standard deviation of the orography. The standard deviation is computed from the Navy 10 minute by 10 minute orography data by taking departures from the mean orography of the model grid. As in other studies the computed h is constrained to 400 m for numerical stability. This constraint can be justified on the assumption that the Coriolis acceleration is at least one order of magnitude larger than the acceleration due to gravity wave drag (see Helfand *et al.* 1987).

As shown by Eliassen and Palm (1961) $\vec{\tau}_{gw}$ is independent of height in the absence of turbulent dissipation or transience. In such a case the parameterization deposits the momentum in the top layer of the model and hence there is no body force on the atmosphere in the remaining lower layers because $\partial \vec{\tau}_{gw}/\partial\sigma = 0$ in equation (3.1)

On the other hand, the value of $\vec{\tau}_{gw}$ does change in the vertical when the local value of the wave-modified Richardson number, $\mathbf{R}_{im} = \mathbf{R}_i(1 - F_r)$, is less than or equal to one quarter. Wave breaking occurs at levels where amplification of the wave causes the local Froude number to exceed a critical Froude number, $F_{rc} = (1 - 1/4\mathbf{R}_i)$. If such a condition is met the wave saturation hypothesis of Lindzen (1981) is invoked and wave–induced turbulence reduces the magnitude of $\vec{\tau}_{gw}$. Finally, $\vec{\tau}_{gw}$ vanishes when a critical level, convective instability, or shear instability is encountered. Critical levels are where $\vec{V} \cdot \vec{V}_{surface} \leq 0$. Shear instabilities, $\mathbf{R}_i < \frac{1}{4}$, create turbulence and according to Eliassen and Palm (1961) the momentum flux vanishes at the level. In order to allow the gravity wave effects to propagate above the base layer it is assumed that $\vec{\tau}_{gw}$ can change in the base layer only due to wave saturation and not by the occurrence of critical levels or instabilities.

4. Experiments and results

We have integrated the model for thirty days both with and without the GWD starting with initial conditions in January and July. There are three 30–day winter forecast starting on January 7, 1990 12Z, January 8, 1990 00Z, and January 8, 1990 12Z. However, the impact of the GWD was independent of the 12 hour difference in the initial conditions. Consequently, we have assumed that one integration of the model is sufficient with a July initial condition. The model was integrated for thirty days starting on July 15, 1989 00Z. In all eight integrations National Meteorological Center (NMC) analyses were used for the initial conditions and for verifying the extended range forecasts. Throughout the following sections we shall refer to the forecasts without the GWD as the control and NMC analysis minus control as the "error". The difference between the forecasts with and without the GWD will be referred to as the "corrections".

a) Impact of gravity wave drag on temperature

Much of the previous literature was devoted to the impact on the zonal momentum and because much of the effects on the zonal wind are consistent with the temperature we will focus our attention on the temperature field. Figures 1(a) and 2(a) show the 30–day mean errors in zonal mean temperature (T_z) and Figures 1(b) and 2(b) show the corrections to T_z for the

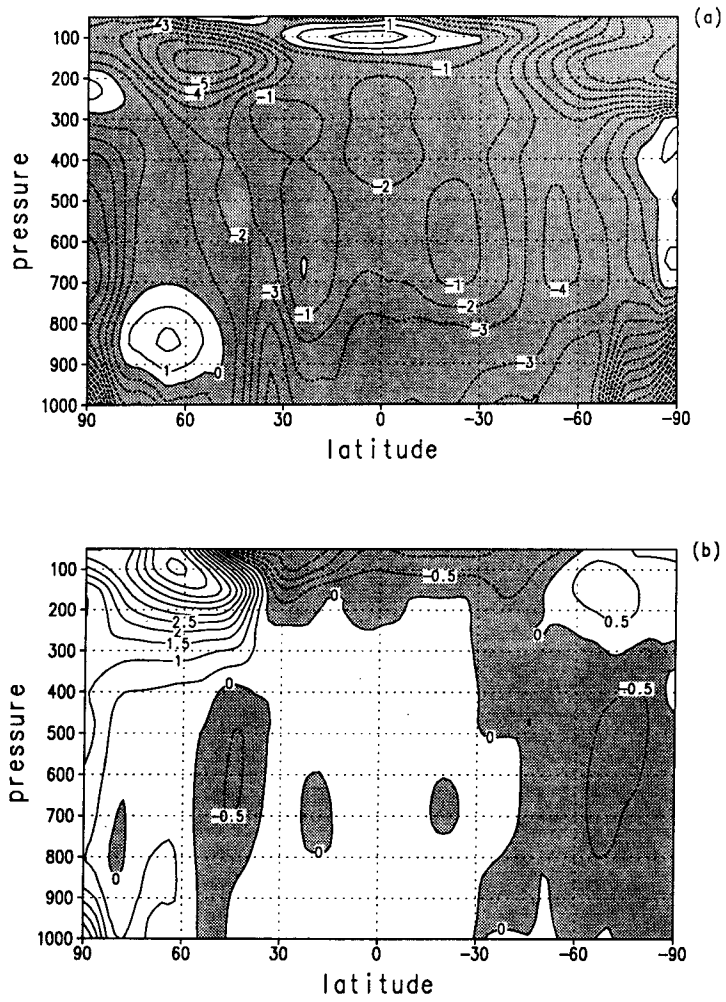

Fig. 1. 30-day mean zonal mean temperature errors and corrections in degrees K; (a) contour interval of 1.0; (b) contour interval of 0.5. Shaded regions correspond to negative values.

January and July cases respectively. In the January forecast, the low temperature bias is present in almost all of the modeled atmosphere with the largest error in the upper levels in the middle and high latitudes. The corrections due to the GWD are largest in the Northern Hemisphere at high latitudes and upper levels particularly poleward of 45°N and above 250 mb. There is also a corresponding small correction in the Southern Hemisphere and a correction to the high temperature bias in the tropical lower stratosphere. All of these corrections are consistent with the corrections made to the zonal winds (not shown). For the July forecast the overall impact is positive; yet there are regions where the GWD increases the temperature bias. There is a positive impact north of 45°N between 300 mb and 50 mb, although the improvement is not as large as in the January case. Below 700 mb and north of 70°N, however, the control forecast agrees better with the analysis than the GWD forecast. In the Southern Hemisphere, the upper tropospheric warming due to the GWD around 50°S partially compensates for the large error in the control integration centered at 30°S and 150 mb. However, this warming also degrades the forecast in significant regions.

The differences in the corrections between the seasons can largely be attributed to the differ-

ences in the control T_z and U_z between the seasons and the difference in the topographic variance between the hemispheres. For instance, in the January forecast for the Northern Hemisphere the strength of the zonal wind is significantly larger than in the July forecast; thus the dissipative effects of the wave drag must also be larger. The drag in the Southern Hemisphere in July is half that of the Northern Hemisphere in January because of the larger topographic variance in the Northern Hemisphere. On the other hand, some of the more subtle differences cannot be so easily explained. In the July forecast the upper topographic warming due to the drag is substantially poleward of the largest low temperature error in both hemispheres. At the North Pole in July below 300 mb the GWD effect almost doubles the low temperature errors observed in the control integration. These large low level temperature effects are not observed in the January GWD forecast.

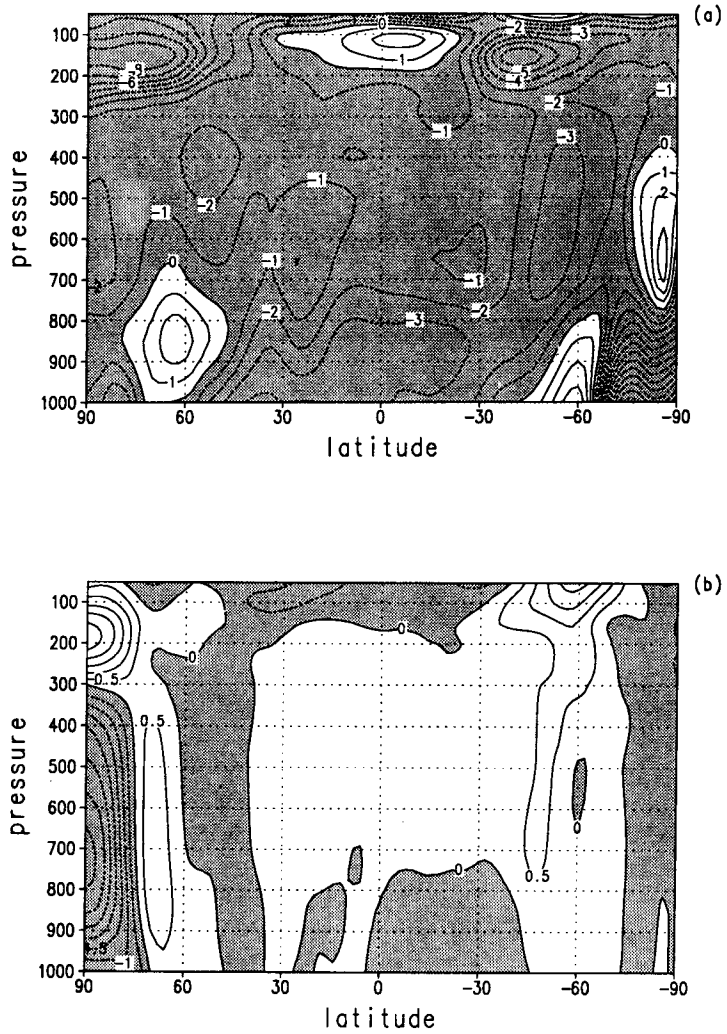

Fig. 2. Same as Fig. 1 except for the July forecast. Shaded regions correspond to negative values.

The geographical distributions of the 150 mb temperature errors and corrections for the January and July integrations respectively are presented in Figures 3 and 4. The regional low bias covers a substantial portion of the Northern Hemisphere north of 30°N. There is a high

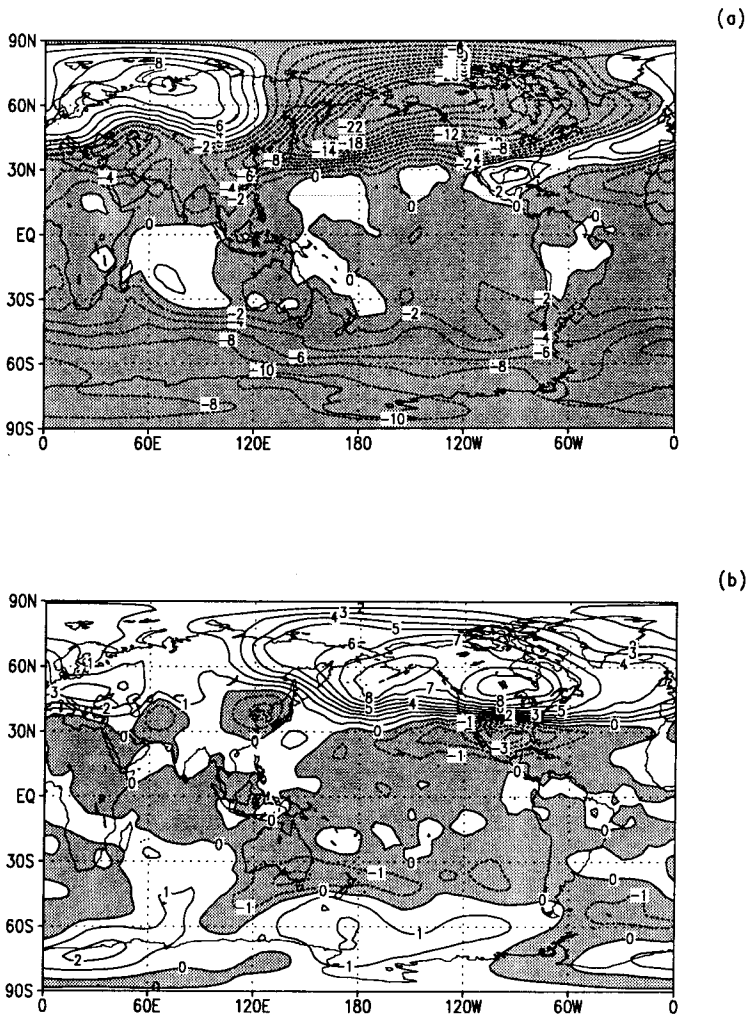

Fig. 3. 30-day mean 150 mb temperature errors and corrections for the January forecast in degrees K; (a) errors, contour interval of 2.0; (b) corrections, contour interval of 1.0. Shaded regions correspond to negative values.

bias in the Northern Hemisphere over much of Eurasia and a low bias at all latitudes poleward of 30°S. The GWD reduces the low bias over North America by as much as 50%. There is also some improvements south of 30°N centered over Mexico. The GWD has no effect on the high bias over Eurasia and the low bias in the Southern Hemisphere polar latitudes is reduced to some small extent. The GWD also increases the excessively low temperatures in the July forecast. The low bias just off the coast of Chile is reduced by 50% but the low temperature errors are enhanced east of 30°E. In the Northern Hemsiphere throughout much of the polar latitudes the GWD reduces the temperature error by as much as 2°K. On the other hand, there are also regions where GWD increases the error: Central Eurasia and Western Europe for example, where the GWD increases the temperature error by as much as 2°K.

Several previous studies (see Vernekar *et al.*, 1992 and Helfand *et al.*, 1987) have shown, using global skill score statistics, that the effect of the GWD is only detectable beyond day–5 of the forecasts. These results have lead several authors (Palmer *et al.*, 1986 and Helfand *et al.*, 1987)

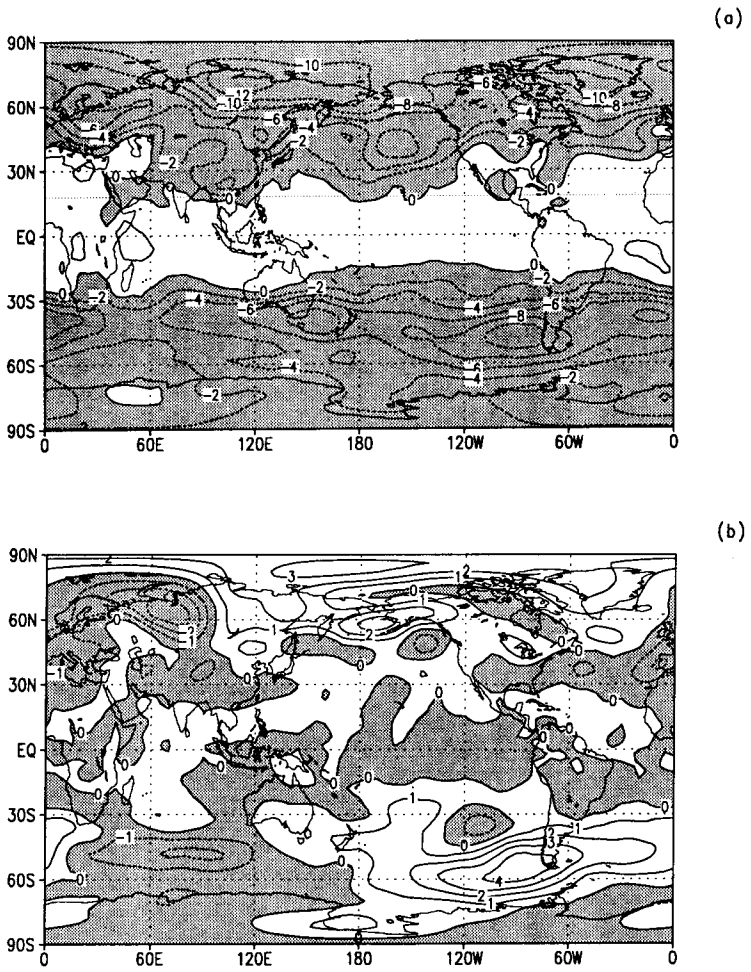

Fig. 4. Same as Fig. 3 except for the July forecast; (a) contour interval of 1.0; (b) contour interval 0.5. Shaded regions correspond to negative values.

to argue that it takes five to seven days before the wave drag effects can be detected. Figure 5 shows the zonally averaged absolute temperature averaged over the regions 45°N – 90°N and from 400 mb to the top of the model for the control case, the GWD case and NMC analyses as a 30–day time series for the January integration. Clearly the impact of the forecast is felt immediately. Most of the errors in the control integration is restricted to the first seven days. The rapid cooling of the first seven days is almost completely eliminated by including the GWD effects. By day–20 the regionally averaged temperatures for the GWD forecast and the control forecast are in phase but the control integration is in excess of 2°K colder.

b) Impact of gravity wave drag on sea level pressure

Figures 6 and 7 present the 30-day mean sea level pressure errors and corrections for the January and July cases respectively. In January there is a high negative correlation between the error in the control integration (Fig. 6a) and the GWD correction (Fig. 6b) implying a strong positive impact of the GWD. The largest areas of improvement include the Northern Hemisphere high latitudes extending over both the North American and Eurasian continents which is consistent with the temperature field. In addition, the correlation appears high over mountainous regions particularly the Himalayan mountains but also the Rocky mountains. There are, of course, areas of negative impact such as in the vicinity of the Aleutian low. There is a large positive error centered over Iceland in which the GWD has little or no impact. In the Southern Hemisphere there is also a general overall improvement of the forecast of the monthly mean with the greatest impact in the polar latitudes where the GWD reduces the sea level pressure error by 50%. The increased drag effects systematically enhances the sea level pressure at the North Pole and reduces the sea level pressure at the South Pole. This redistribution of mass is accomplished by enhanced divergent circulations.

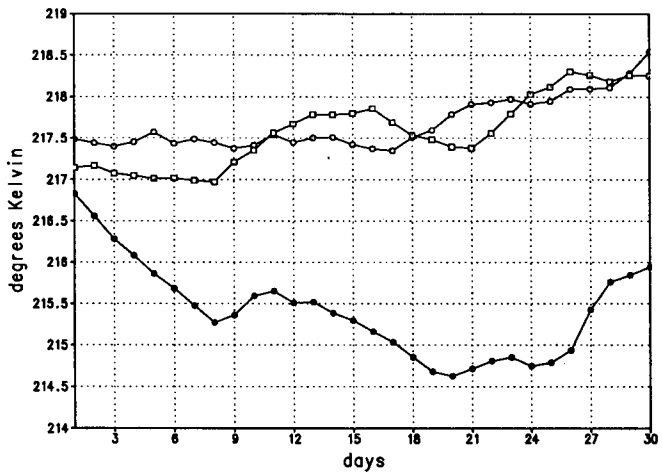

Fig. 5. The January forecast zonally averaged absolute temperature averaged over the region 45°N to 90°N and from 400 mb to the top of the model. Open circles correspond to the NMC analysis, filled circles correspond to the control forecast and open squares indicate the GWD forecast.

The dissipative effects of the GWD on the momentum requires an adjustment in the north-south temperature gradient which requires a meridional transfer of mass. This transfer of mass tends to increase the sea level pressure in the high latitudes of the Northern Hemisphere and reduces the sea level pressures in the high latitudes of the Southern Hemisphere. In the January forecast it is clear that in the control case there is too much mass accumulating in the tropics and too little mass accumulating in the Northern Hemisphere middle and high latitudes. Moreover, in the Southern Hemisphere polar latitudes too much mass has accumulated. The GWD modifies the distribution of mass throughout the globe and improves the forecast. From the equator to 30°N the agreement between the GWD case and the NMC analysis is close. In the middle latitudes of the Northern Hemisphere mass tends to over accumulate slightly in the GWD case;

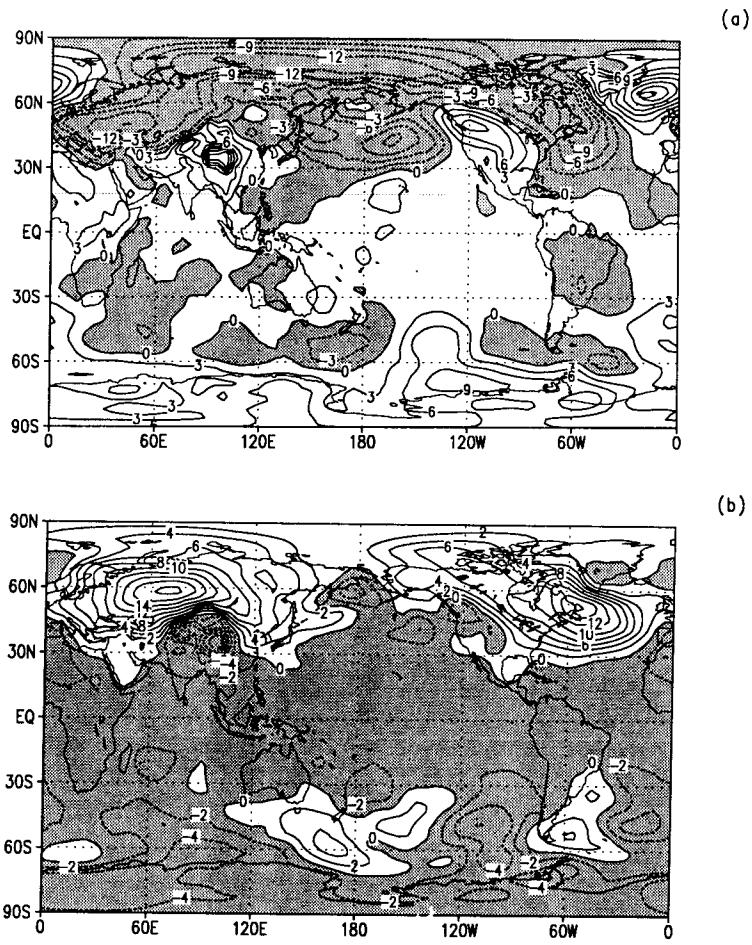

Fig. 6. Same as Fig. 3 except for sea level pressure in mb; (a) contour interval of 3.0; (b) contour interval of 2.0. shaded regions correspond to negative values.

however, the mass distribution in the GWD case is nevertheless an improvement over the control case. The distribution of mass in the polar latitudes of both hemispheres is improved by including the GWD in the forecast.

In the July forecast (Fig. 7) the impact of the GWD is again positive. In particular the GWD improves the forecast near the Southern pole where the model produces sea level pressures that are much too high. The GWD corrects these errors by up to 50%. The corrections in the Northern Hemisphere are relatively small; however, the general character of the correction is an overall improvement in the July forecast of the sea level pressure. Consistent with the temperature field the impact of the GWD appears somewhat weaker in July. Furthermore, the correlation between Figures 6(a) and 6(b) is -.50 for the winter hemisphere indicating a net positive impact but the correlation between Figures 7(a) and 7(b) is -.42 for the winter hemisphere. This implies that the enhanced drag effect improves the January forecast slightly more than the July forecast.

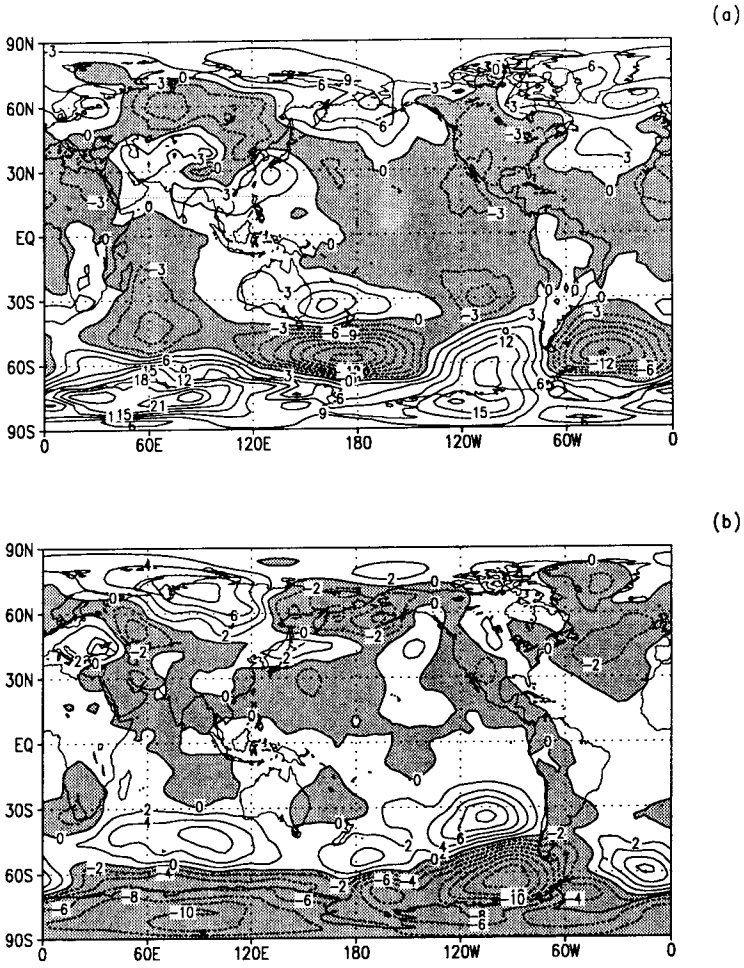

Fig. 7. Same as Fig. 6 except for the July forecast.

c) Impact of gravity wave drag on the divergence field

As mentioned in the Introduction, Smith (1979) speculated that the mean meridional circulations, that is, the divergent motion will be enhanced in order to bring the momentum lost by the large scale flow to the ground to be dissipated. While Smith's (1979) reasoning seems quite plausible the magnitude of the enhanced divergent motions has not been previously assessed. The previous sections have clearly demonstrated how the GWD effects greatly influence the monthly mean forecast in the middle and high latitudes. However, in the temperature and the sea level pressure it was difficult to detect a response in the low latitudes. The following analysis of the divergent circulations both determines the magnitude of the enhanced mean meridional motion and the impact of the GWD in the tropics. The mean meridional circulations and the changes induced by the GWD for the January and July cases are presented in Figures 8 and 9 respectively. The meridional stream function, ψ, is imputed by setting $v_z = (-g/2\pi a \cos\phi)\frac{\partial \psi}{\partial p}$ and $\omega_z = (g/2\pi a^2 \cos\phi)\frac{\partial \psi}{\partial \phi}$, where ω_z and v_z have been zonally and time averaged. The convection here is that negative centers correspond to clockwise circulations and positive centers

correspond to counter clockwise circulations. The model simulates, in both January and July, the qualitative nature of the seasonal positions of the Hadley and Ferrel cells quite well.

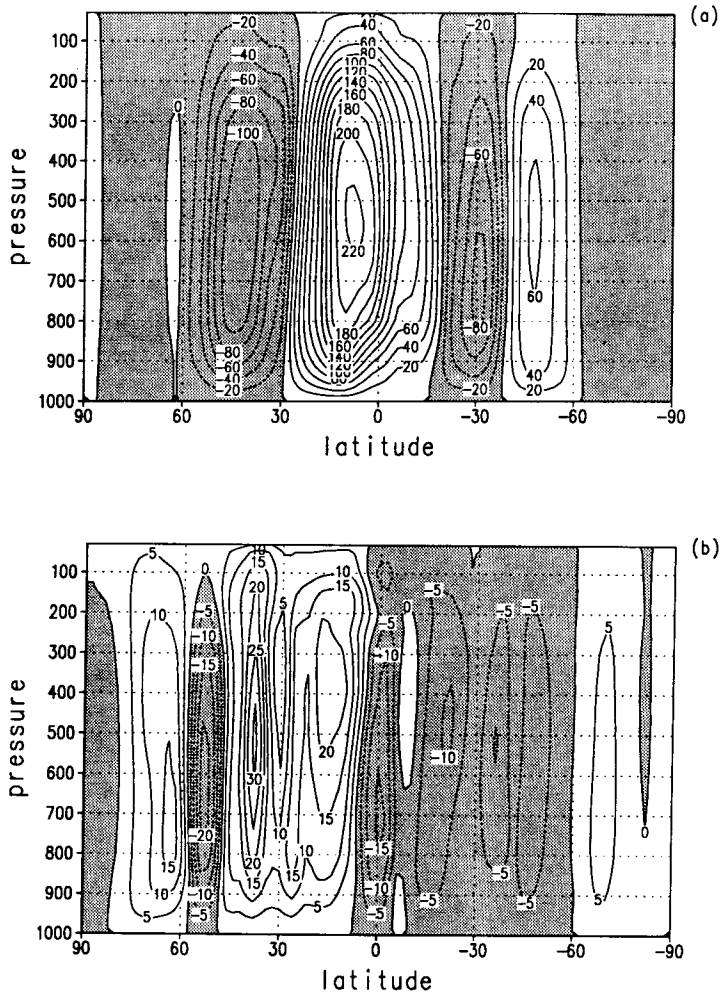

Fig. 8. 30-day average mean meridional stream function for January in 10^9 kg sec^{-1}; (a) control forecast, contour interval of 20.0; (b) GWD forecast minus control forecast, contour interval of 5.0. Shaded regions correspond to negative values.

In January, Figure 8, the GWD influences both the Hadley and Ferrel cells. The Hadley cell shifts northward with an intensification of the rising branch but a weakening of the descending branch. This leads to increases in zonal mean precipitation at the latitude bands 10°S to 30°S and 10°N to 30°N. The inter-tropical convergence zone (ITCZ) in January intensfies in both hemispheres. Although not shown here, there is a 5% increase in precipitation in these narrow latitude bands. In the latitude band 45°N to 55°N there is an increase in descending motion corresponding to the increase in surface pressure in this region. There is also a substantial enhancement of the direct cell in the high latitudes.

In July the GWD dramatically enhances the mass circulation in the Hadley cell by more than fifteen percent; while the impact is significantly smaller in the middle and high latitudes. This enhanced Hadley circulation coincides with sustantial changes in the zonal mean precipitation in the tropics. The zonal mean precipitation from the equator to 20°N increases by 5% and from the equator to 20°S the rainfall decreases by 2.5%. The changes in the distribution of mass in the high latitudes (Fig. 7) can also be connected to changes in the mean meridional motion. For instance, the enhanced rising motions south of 60°S correspond to the decreased sea level pressure in that region. Furthermore, the over-accumulation of mass in the polar latitudes of the Northern Hemisphere can be detected in the increased descending motion at these latitudes. In the middle and high latitude the impact of the GWD was strongest in January, but in the tropics the impact was strongest in July.

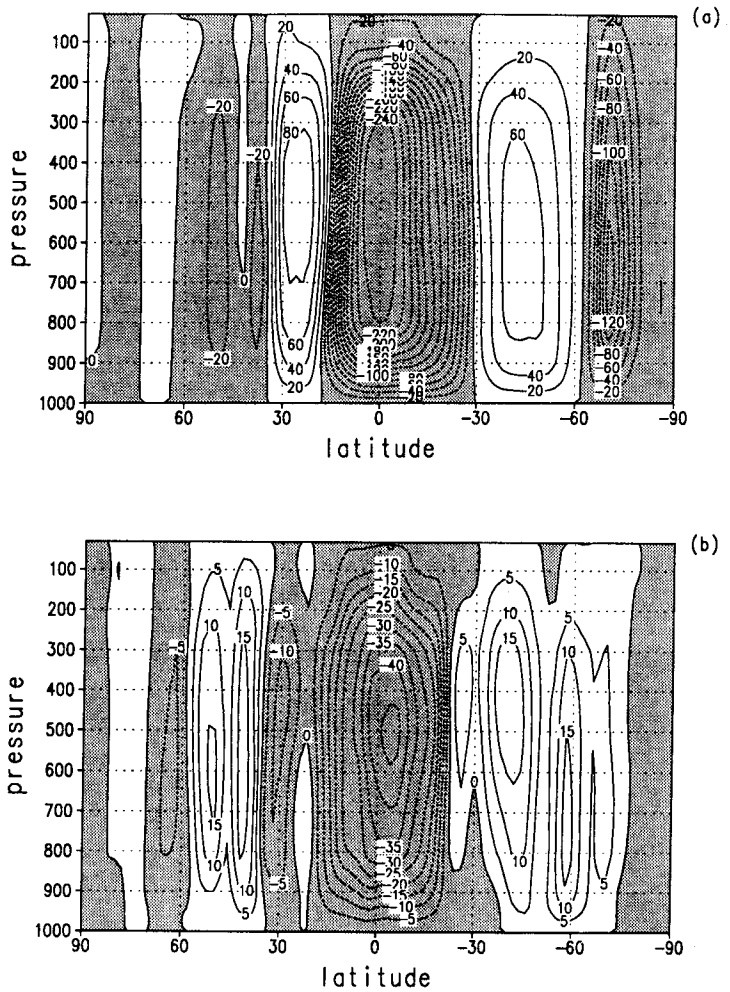

Fig. 9. Same as Fig. 8 except for the July forecast; (a) contour interval of 20.0; (b) contour interval of 5.0. Shaded regions correspond to negative values.

Asocciated with the changes in the mean meridional motions are changes in the irrotational part of the wind and corresponding changes in the precipitation field. Figures 10(a) and 11(a) show the 200 mb velocity potential difference (GWD case minus control case) and the superimposed divergent wind difference for the January and July cases respectively. The second panels,

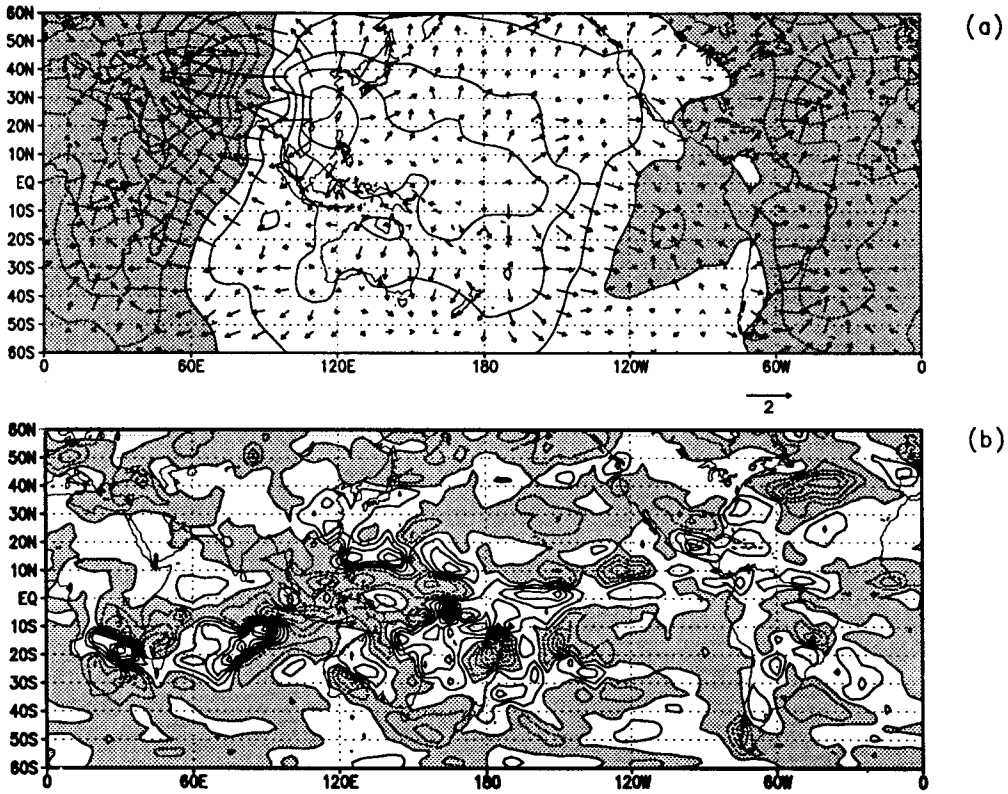

Fig. 10. (a) January 30-day mean 200 mb velocity potential (10^{-4} m^2 sec^{-1}) and divergent wind (m sec^{-1}) difference (GWD forecast minus control forecast), contour interval is 5×10^5; (b) January 30-day mean precipitation difference (GWD forecast minus control forecast) in mm day^{-1}, contour interval of 1.0. Shaded regions correspond to negative values.

Figs. 10(b) and 11(b) show the precipitation differences. Areas of increased convergence at 200 mb associated with increased divergence at lower levels are correlated with areas of decreased precipitation as can be seen from these figures. Areas of increased divergence at 200 mb are correlated with increased precipitation. The changes in precipitation are most dramatic in the July integration where precipitation is increased by as much as 7.5 mm day^{-1} in the active areas of convection. The rain has increased in the northern tropics and decreased in the southern tropics as was expected from the enhancement of the Hadley circulation. In the January case the most striking difference is in the middle latitudes of the Northern Hemisphere where in the zonal average the increase in convergence out weighs the increase in divergence resulting in a net decrease in the zonally averaged precipitation. This result, as expected, is entirely consistent with the changes in the mean meridional motions.

The effect of the GWD is to modify the magnitude of the rate of precipitation, but it does not create new centers of precipitation. In both January and July the global mean precipitation increases because of the enhanced divergent motions. We cannot adequately verify whether the GWD actually improves the forecast of the monthly mean precipitation in the tropics. However, because this GCM, not unlike most other GCMs, tends to underestimate global mean precipitation we believe the tendency due to GWD is in the appropriate direction.

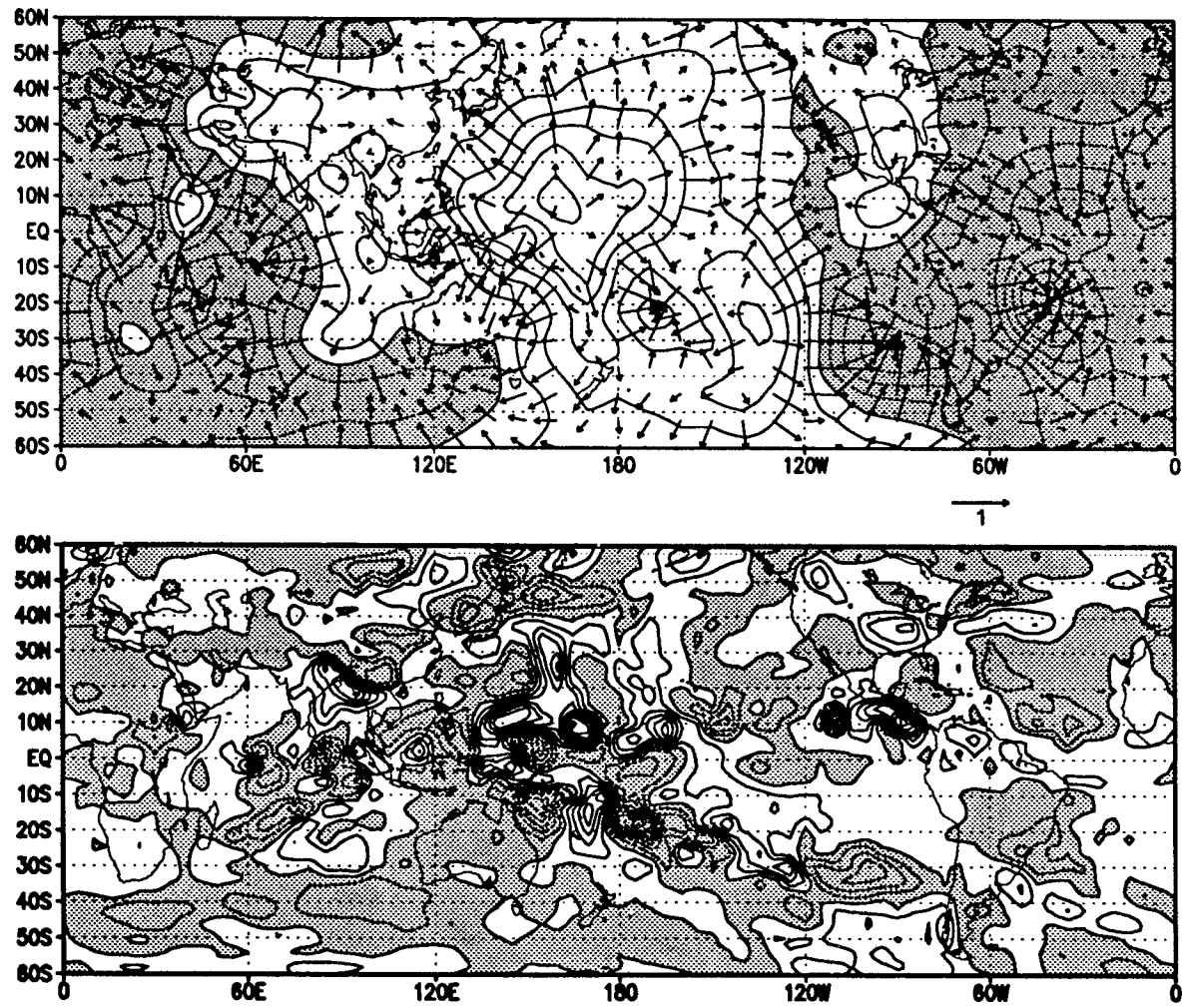

Fig. 11. Same as Fig. 10 except for the July forecast.

The secondary circulations or divergent circulations are greatly enhanced by the GWD. Figures 12(a) and 13(a) present the globally averaged kinetic energy of the irrotational component of the flow as a function of pressure and time for the January and July cases without the GWD effects. Figures 12(b) and 13(b) show the difference between the GWD case and the control case for the corresponding months. Beyond day-15 in both cases there is a significant increase in the kinetic energy of the irrotational flow by as much as 30% at the maximum jet level. The kinetic energy of the rotational motion (not shown here), however is reduced by less than 1%. This reduction is atributed to the dissipation effects of the GWD. The enhanced divergent circulations are consistent with enhanced conversion of available potential energy to kinetic energy of the irrotational motion. This conversion term increases when there is an increase in warm air rising and cold air sinking associated with increased convection. The enhanced Hadley cell (Figs. 8(b) and 9(b)) will convert the available potential energy to kinetic energy of the irrotational motion.

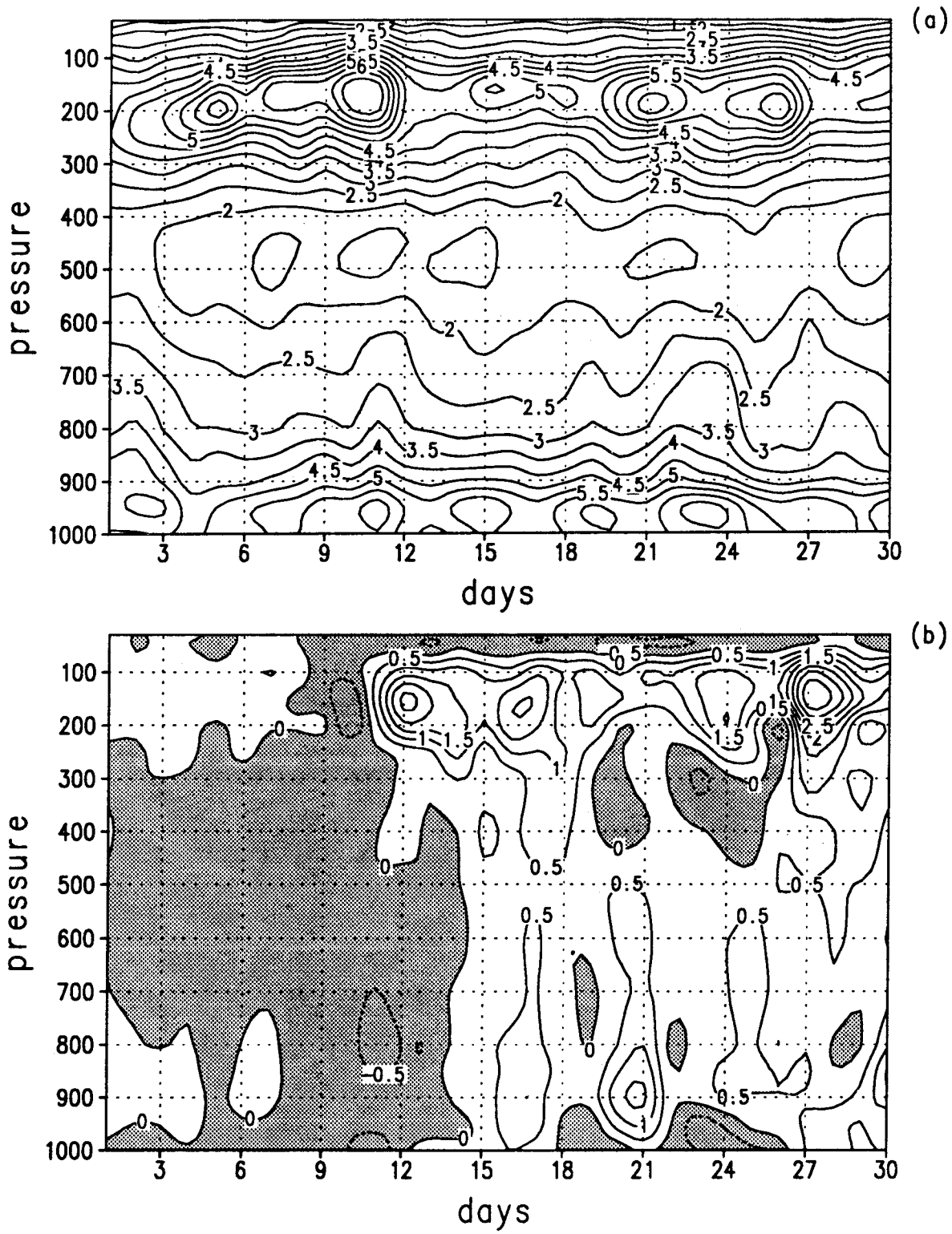

Fig. 12. January irrotational kinetic energy in m^2 sec^{-2}; (a) control forecast, contour interval of 0.5; (b) GWD forecast minus control forecast, contour interval of 0.5. Shaded region correspond to negative values.

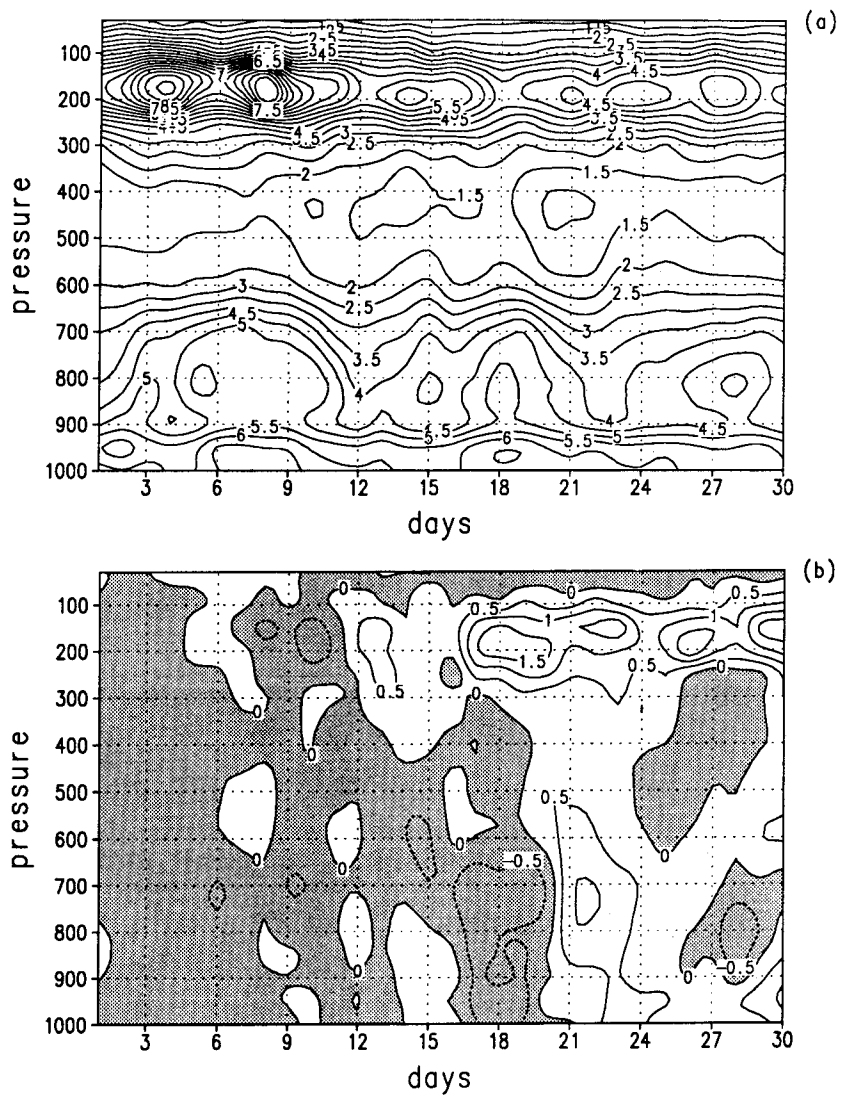

Fig. 13. Same as Fig. 12 except for the July forecast.

5. Summary and conclusions

A GWD parameterization scheme accounting for non-linear effects at the surface was incorporated into a state-of-the-art GCM. The vertical variation of the drag depends on conditions for wave saturation and instabilities. Two pairs of 30-day forecasts were evaluated, one pair initialized in January and the other in July. Within each pair, forcasts were made both with and without the GWD effects. The impact of the GWD on extended range forecasts in the middle and high latitudes was investigated in terms of the temperature and sea level pressure fields. In the tropics the enhanced secondary circulations as well as the associated changes in precipitaion was assessed.

We have shown that the GWD effects improve the extended range forecasts for January and July particularly in the winter hemisphere. Global skill scores (not shown) indicate GWD

improvements for the entire 30 days in both January and July. Unfortunately, a large portion of the improvements occur beyond the time when the instantaneous forecasts are useful. In terms of the monthly mean forecast the GWD provides a systematic improvement in both January and July. The GWD effects reduce the westerly bias in the zonal wind forecast and the low bias in the temperature forecast. The impact of the GWD effects are clearly evident in the regionally averaged temperature field by day-1. As a consequence of changes in momentum and temperature there is a meridional mass transport such that forecast of monthly mean sea level pressures are improved particularly in the polar regions. Increased dissipation of momentum by the GWD enhances mean meridional motions by as much as 15% and the kinetic energy of the divergent motions increases by about 30% beyond day-15. These enhanced secondary circulations are consistent with enhanced conversion of available potential energy to kinetic energy. The increased conversion is accomplished when there is an increase in relatively warm air rising and relatively cold air sinking which is directly observed in the mean meridional motions. The enhanced secondary circulations can be directly linked to changes in precipitation with increased precipitation in the summer hemisphere and decreased precipitation in the winter hemisphere in July and increased precipitation along the ITCZ in January. In the middle and high latitudes the impact of the GWD is largest in January. In the tropics the largest effects are felt in July.

These conclusions are based on only two 30-day forecasts; yet the impact of the GWD on this model appears quite robust. Two other 30-day forecasts initialized on Jan. 7, 1990 12Z and Jan. 8, 1990 12Z showed similar impacts. Furthermore, in an earlier study (Vernekar *et al.*, 1992) four forecasts were made in order to determine the impact of the GWD on medium range forecasts. The results of these medium range forecasts are consistent with the extended range forecasts described above and show a positive impact in all four cases.

There are, however, some limitation to this study that need to be mentioned. While the magnitude of the GWD effects is reasonable there is a degree of arbitrariness in the values of ℓ^*, the wave length of the monochromatic wave and h, the orographic standard deviation constrained to 400 m. The GWD effects also depend on the orientation of the mountains and wind directions (Miller and Palmer, 1986). The parameterization includes the implicit effects of moisture through the use of virtual temperature in determining the Brunt-Vaisala frequency. The explicit effects of moisture (condensation) are not included here. Surgi (1989) included the explicit effects of moisture on the Brunt-Vaisala frequency and the effect of moisture condensation. However, the impact of this parameterization on the FSU (Florida State University) model was not much different from the results presented here or any other similar studies.

Acknowledgements

We wish to thank E. Schneider, J. Shukla and J. Kinter for helpful discussions and comments. We are grateful to L. Marx and M. Fennessy for providing their time generously for consultations on the COLA model. We would also like to thank B. Doty for the use of his graphics software (GRADS) in preparing the figures. The integrations were performed on the NASA Goddard CRAY-YMP, Greenbelt, Maryland. This research was partly supported by NSF grant ATM-8708170, NSF grant ATM-8912576 and AFGL grant F19628-88-K-0015.

REFERENCES

Alpert, J. C., M. Kanamitsu, P. M. Caplan, J. G. Sela, G. H. White and E. Kalnay, 1988. Mountain induced gravity wave drag parameterization in the NMC medium-range forecast model. Proceedings of the Eight Conference on Numerical Weather Prediction, Baltimore, Maryland, February 22-26, 1988, 726-733.

Boer, G. J., N. A. McFarlane, R. Laprise, J. D. Henderson and J. -P. Blachet, 1984. The Canadian Climate Centre Spectral Atmospheric General Circulation Model. *Atmos. Ocean.*, **22**, 397-429.

Bretherton, F. P., 1969. Momentum transport by gravity waves. *Quart. J. Roy. Meteor. Soc.*, **95**, 213-243.

Brown, P. R. A., 1983. Aircraft measurements of mountain waves and their associated momentum flux over the British Isles. *Quart. J. Roy. Meteor. Soc.*, **109**, 849-865.

Eliassen, A. and E. Palm, 1961. On the transfer of energy in stationary mountain waves. *Geofys. Publ.*, **22**, 1-23.

Harshvardhan, R. Davis, D. A. Randall and T. G. Corsetti, 1987. A fast radiation parameterization for general circulation models. *J. Geophys. Res.*, **92**, 1009-1016.

Helfand, H. M., J. C. Jusem, J. Pfaendtner, J. Tenenbaum and E. Kalnay, 1987. The effect of a gravity wave drag parameterization on GLA fourth order GCM forecasts. *Short and Medium-Range Numerical Weather Prediction Collection of Papers Presented at the WMO/IUGG NWP Symposium*, Tokyo, 4-8 August, 1986.

Hoinka, K. P., 1984. Observations of a mountain wave event over the Pyrenees. *Tellus*, **36A**, 369-383.

Iwasaki, T., S. Yamada and K. Tada, 1989. A parameterization scheme of orographic gravity wave drag with two different vertical partitionings. Part I: Impact on medium-range forecasts. *J. Meteor. Soc. Japan*, **67**, 11-27.

Kinter, III J. L., J. Shukla, L. Marx and E. Schneider, 1988. A simulation of winter and summer circulation with the NMC global spectral model. *J. Atmos. Sci.*, **45**, 2468-2522.

Kuo, H. L., 1974. Further studies of the parameterization of the influence of cumulus convection on large-scale flow. *J. Atmos. Sci.*, **31**, 1232-1240.

Lilly, D. K., 1972. Wave momentum flux: A GARP problem. *Bull. Amer. Meteor. Soc.*, **20**, 17.

Lilly, D. K., J. M. Nicholls, R. M. Chervin, P. J. Kennedy and J. B. Klemp, 1982. Aircraft measurements of wave momentum flux over the Colorado Rocky Mountains. *Quart. J. Meteor. Soc.*, **108**, 625-642.

Lindzen, R. S., 1981. Turbulence and stress due to gravity wave tidal breakdown. *J. Geophys. Res.*, **86**, 9707-9714.

McFarlane, N. A., 1987. The effect of orographically excited gravity wave drag on the general circulation of the lower stratosphere and troposphere. *J. Atmos. Sci.*, **44**, 1775-1800.

Mellor, G. L. and T. Yamada, 1982. Development of a turbulence closure model for geophysical fluid problems. *Rev. Geophys. Space Phys.*, **20**, 851-875.

Miller, M. J. and T. N. Palmer, 1986. Orographic gravity wave drag: its parameterization and influence in general circulation and numerical weather prediction models. ECMWF Seminar/Workshop 1986 on Obervations, Theory and Modeling of Orographic Effects, Reading, Eng., September 15-20, 1986.

Miyakoda, K. and J. Sirutis, 1990. Subgrid scale physics in 1-month forecasts. Part II: Systematic error and blocking forecasts. *Mon. Wea. Rev.*, **118**, 1065-1081.

Palmer, T. N., G. J. Shutts and R. Swinbank, 1986. Alleviation of a systematic westerly bias in general circulation and numerical weather prediction models through an orographic gravity wave drag parameterization. *Quart. J. Roy. Meteor. Soc.*, **112**, 1001-1039.

Pierrehumbert, R. T., 1987. An essay on the parameterization of orographic gravity wave drag. Geophysical Fluid Dynamics Laboratory/NOAA/Princeton University, Princeton, N. J. 08542,

Sato, N., P. Sellers, D. Randell, E. Schneider, J. Shukla, J. Kinter, Y. -T. Hou and E. Albertazzi, 1989. Effects of implementing a simple biosphere model in a general circulation model. *J. Atmos. Sci.*, **46**, 2757-2782.

Schneider, E. K. and R. Lindzen, 1976. The influence of stable stratification on a thermally driven tropical boundary layer. *J. Atmos. Sci.*, **33**, 1301-1307.

Sela, J. G., 1980. Spectral modeling at the National Meteorological Center. *Mon. Wea. Rev.*, **106**, 1279-1292.

Sellers, P. J., Y. Mintz, Y. C. Sud and A. Dalcher, 1986. A simple biosphere model (SiB) for use within general circulation models. *J. Atmos. Sci.*, **43**, 505-531.

Slingo, J. M., 1980. A cloud parameterization scheme derived from GATE data for use in a numerical model. *Quart. J. Roy. Meteor. Soc.*, **106**, 747-770.

Slingo, J. M., 1987. The development and verification of a cloud prediction scheme for the ECMWF model. *Quart. J. Roy. Meteor. Soc.*, **113**, 899-927.

Smith, R. E., 1979. The influence of mountains in the atmosphere. *Adv. Geophysics*, **21**, 87-230.

Smith, R. E., 1978. A measurement of mountain drag. *J. Atmos. Sci.*, **35**, 1644-1654.

Sirutis, J. and K. Miyakoda, 1990. Subrid scale physics in 1-month forecasts. Part I: experiment with four parameterization packages. *Mon. Wea. Rev.*, **118**, 1043-1064.

Stern, W. F. and R. T. Pierrehumbert, 1988. The impact of an orographic gravity wave drag parameterization on extended range prediction with a GCM. Proceedings of the Eight Conference on Numerical Weather Prediction, Baltimore, Maryland, February 22-26, 1988, 745-750.

Surgi, N., 1989. Systematic errors of the FSU global spectral model. *Mon. Wea. Rev.*, **117**, 1751-1766.

Tiedtke, M., 1984. The effect of penetrative cumulus convection on large scale flow in a general circulation model. *Beitr. Phys. Atmos.*, **57**, 216-239.

Vernekar, A. D., B. Kirtman, D. DeWitt and J. Zhou, 1992. Orographic gravity-wave drag effects on medium-range forecasts with a general circulation model. *Physical Processes in Atmospheric Models.* Edited by D. R. Sikka and S. S. Singh. Wiley Eastern Limited, 295-307.